Mechanics of Living Cells Measured by Laser Tracking Microrheology

Soichiro Yamada,* Denis Wirtz,* and Scot C. Kuo†

*Department of Chemical Engineering, The Johns Hopkins University, Baltimore, Maryland 21218; and †Department of Biomedical Engineering, The Johns Hopkins University, Baltimore, Maryland 21205 USA

ABSTRACT To establish laser-tracking microrheology (LTM) as a new technique for quantifying cytoskeletal mechanics, we measure viscoelastic moduli with wide bandwidth (5 decades) within living cells. With the first subcellular measurements of viscoelastic phase angles, LTM provides estimates of solid versus liquid behavior at different frequencies. In LTM, the viscoelastic shear moduli are inferred from the Brownian motion of particles embedded in the cytoskeletal network. Custom laser optoelectronics provide sub-nanometer and near-microsecond resolution of particle trajectories. The kidney epithelial cell line, COS7, has numerous spherical lipid-storage granules that are ideal probes for noninvasive LTM. Although most granules are percolating through perinuclear spaces, a subset of perinuclear granules is embedded in dense viscoelastic cytoplasm. Over all time scales embedded particles exhibit subdiffusive behavior and are not merely tethered by molecular motors. At low frequencies, lamellar regions (820 ± 520 dyne/cm^2) are more rigid than viscoelastic perinuclear regions (330 ± 250 dyne/cm^2, $p < 0.0001$), but spectra converge at high frequencies. Although the actin-disrupting agent, latrunculin A, softens and liquefies lamellae, physiological levels of F-actin, alone (11 ± 1.2 dyne/cm^2) are ~70–fold softer than lamellae. Therefore, F-actin is necessary for lamellae mechanics, but not sufficient. Furthermore, in time-lapse of apparently quiescent cells, individual lamellar granules can show ~4-fold changes in moduli that last >10 s. Over a broad range of frequencies (0.1–30,000 rad/s), LTM provides a unique ability to noninvasively quantify dynamic, local changes in cell viscoelasticity.

INTRODUCTION

Because a major function of cytoskeletal filaments is to support cell structure, mechanical characterization of living cells must complement characterization of reconstituted networks. Despite many plausible molecular mechanisms for controlling cytoskeletal structure, current biophysical methods lack the speed and resolution to monitor mechanics in living cells and cannot adequately test molecular models. To address these shortcomings, we have developed a new approach to cellular mechanics, laser-tracking microrheology (LTM), that quickly characterizes mechanical properties over an ~5-decade range of frequencies. For model polymers, LTM quantitatively provides the same viscoelastic spectra as mechanical rheometry (Mason et al., 1997b).

To measure cell mechanics, cells have been deformed by many techniques. Whole-cell deformations have used a torsional pendulum (e.g., Eichinger et al., 1996), parallel plates (e.g., Thoumine and Ott, 1997), and micropipette aspiration (see Hochmuth, 1993). Smaller mechanical probes of cells include microneedles (e.g., Felder and Elson, 1990; Nicklas, 1983), cell poker (e.g., Petersen et al., 1982) and atomic force microscopy (e.g., Radmacher et al., 1996; A-Hassan et al., 1998). Magnetic forces have been applied to particles within living cells (Bausch et al., 1999; Valberg and Albertini, 1985; Crick and Hughes, 1950), and attached to the surface of living cells (Bausch et al., 1998; Wang et al., 1993). So far, optical forces have only been applied to deforming soft subcellular structures, such as the plasma membrane (Kuo and Sheetz, 1992; Schmidt et al., 1993). Mechanical measurements using direct deformations are slow and often invasive. Deformations can be so large as to be nonlinear and, hence, relevant to only situations mimicking the measurement protocol. Furthermore, these approaches often rely upon curve-fit models to extract values of phenomenological springs and dashpots.

Without resorting to phenomenological models, mechanical rheometers can empirically measure mechanical properties over widely varying frequencies. By using large amounts of sample material, such devices can apply very small, linear strains through oscillating surfaces. The resulting viscoelastic shear modulus, G^*, is a complex number that varies with the frequency of oscillation. Its magnitude, G_d ($= |G^*|$), is the material's resistance to deformation, and its phase angle, δ ($= \angle(G^*)$) is an index of the material's solid-like ($\delta = 0$) or liquid-like ($\delta = \pi/2$) behavior. Mechanical rheometers have provided thorough characterization of reconstituted F-actin networks (e.g., Xu et al., 1998b; Janmey et al., 1994). However, mechanical data of comparable quality are not available for living cells.

LTM quantitatively provides the same viscoelastic spectra as mechanical rheometry (Mason et al., 1997b). Unlike mechanical rheometry, no external forces are applied to the material. Instead, mechanical properties are derived from the Brownian motion of individual spherical particles embedded in the viscoelastic material. Unlike percolating particles, embedded particles appear almost stationary and only move distances that are a fraction of their radii. In cytoskeletal networks, the motions of small percolating particles have been used to quantify pore size and "microviscosity" of the solution between the filaments (e.g., Hou et al., 1990; Luby-Phelps et al., 1986). For large particles embedded in

Received for publication 20 July 1999 and in final form 23 December 1999.

Scot C. Kuo, Ross Building, Rm. 724, 720 Rutland Ave., Baltimore, MD 21205. Tel.: 410-614-2528; Fax: 410-955-0549; E-mail: skuo@bme.jhu.edu.

0006-3495/00/04/1736/12 $2.00

cytoskeletal networks, particle motions reveal the elasticity of the cytoskeletal mesh itself (Xu et al., 1998a; Palmer et al., 1998, 1999).

To realize its potential beyond reconstituted networks, we use LTM to probe the mechanics of living cells. Unlike measurements using direct deformations, LTM is fast, sensitive, and quantifies liquid versus solid behavior (viscoelastic phase angle). Furthermore, to demonstrate the noninvasiveness of LTM, we chose the cell line COS7 for cellular measurements. COS7 cells have large, flat lamellae and are rich with spherical "granules" that we demonstrate are ideal for probing cytoskeletal mechanics. The mechanical properties of COS7 cytoplasm are highly heterogeneous, but elasticity generally correlates with F-actin staining. Lamellae are most rigid, but are ~70-fold more rigid than reconstituted F-actin alone. By monitoring lamellar particles, we show that their local mechanics are dynamic and that actin-disrupting agents act quickly to soften moduli. Clearly, F-actin is necessary, but not sufficient, for creating rigid lamellae in living cells.

METHODS

Cell culture

COS7 cells (ATCC CRL-1651) were cultured at 37°C in 5% CO_2 in Dulbecco's Minimal Essential Medium without phenol red supplemented with 10% FBS, 2 mM glutamine, and 25 mM HEPES (Life Technologies Inc., Gaithersburg, MD). All measurements were performed at room temperature. Cells were grown on coverslips etched with identifying grids (Bellco Glass Inc., Vineland, NJ) so that the same cells used for laser tracking could be examined by fluorescent staining. Custom flow chambers allowed the introduction of pharmacological agents without disturbing the cell's position on the microscope.

Fluorescent labeling of cytoskeletal networks

For F-actin labeling, cells were fixed in 3% paraformaldehyde in Dulbecco's phosphate-buffered saline (PBS, Life Technologies), extracted with 0.5% Triton X-100 in PBS (Sigma, St. Louis, MO), and F-actin labeled with rhodamine phalloidin (Molecular Probes, Eugene, OR). For vimentin labeling, cells were fixed in 80% methanol and stained with murine monoclonal V9 (Sigma) and rhodamine goat anti-mouse antibodies. All fluorescently labeled cells were mounted in Slowfade Light (Molecular Probes) to minimize photobleaching, and observed with a Zeiss Z-15 filter set and Plan-Neofluar 40× objective on an Axiovert 135 microscope (Carl Zeiss, Thornwood, NY). Images were acquired with a Photometrics PXL-1400 camera controlled by IPLab software (Scanalytics Inc., Fairfax, VA).

Electron microscopy

For electron microscopy, COS7 cells were fixed in 3% glutaraldehyde in PBS. Coverslips were further fixed by 1% osmium tetroxide in 0.1 M cacodylic acid followed by 2% aqueous uranyl acetate. All electron microscopy reagents were purchased from Ted Pella, Inc. (Redding, CA). Specimens were embedded in epoxy resin after a series of dehydrations with ethanol. Hardened blocks were sectioned parallel and perpendicular to the substrate, and stained with 3% aqueous mixture of uranyl acetate and lead citrate. Electron micrographs of epoxy-embedded thin cell sections were obtained using a Zeiss EM10 electron microscope (Carl Zeiss).

Actin preparation

Actin was extracted from rabbit skeletal muscle acetone powder as described by Spudich and Watt (1971). The resulting actin was gel filtered with Sephacryl 300 HR in buffer G (0.2 mM ATP, 0.5 mM dithiothreitol, 0.1 mM $CaCl_2$, 1 mM NaN_3, 2 mM Tris-Cl, pH 8 at 25°C). The concentration of eluted actin was determined spectrophotometrically at 290 nm (MacLean-Fletcher and Pollard, 1980). For particle tracking measurements, actin was polymerized in the presence of 5×10^{-7} (w/v) 1 μm-diameter carboxylated polystyrene particles (Polysciences, Warrington, PA) so that the average distance between particles was ~100 μm. Polymerization was initiated by adding one-tenth volume of 10 × KMEI (500 mM KCl, 10 mM $MgCl_2$, 10 mM EGTA, 100 mM imidazole pH 7 at 25°C), and immediately assembled into the microscope slide chamber. To minimize wall effects, all particles used for laser tracking were at least 10 μm from the coverslip surface.

Laser deflection particle tracking

Using a focused, low-power laser beam, we track a probe particle by monitoring its forward-scattered light with a quadrant photodiode detector (see Fig. 1). Any off-axis motion of the particle deflects energy away from the optical axis and produces imbalances between signals from photodiode quadrants. Laser powers are low (0.13 mW, $\lambda = 670$ nm) so that optical forces are negligible. Built on an Axiovert 100TV microscope (Carl Zeiss), a custom light path for the quadrant photodiode detector was built onto the high numerical aperture (1.4 NA) condenser. Because of its limited aperture, the quadrant photodiode detector is not conjugate to the back aperture of the objective. Photocurrent differences between opposing quadrant pairs are amplified into a voltage that is subsequently digitized by a 16-bit A/D converter (ComputerBoards Inc., Middleboro, MA). Although the analog bandwidth of our photodiode circuitry is ~200 kHz, signals were filtered at 22 kHz to prevent aliasing during digitization.

Calibration of particle displacements and sizes

Laser-tracking signals were calibrated for each probe particle by monitoring the laser signal as a function of the *xy* piezoelectric stage displacement

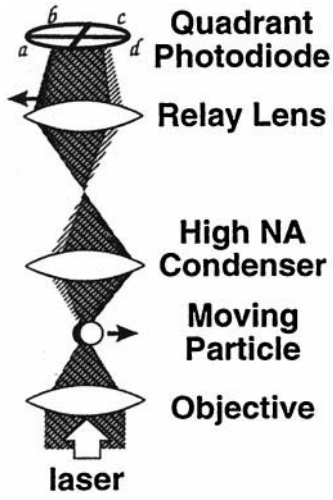

FIGURE 1 Principle of laser deflection particle tracking. A particle at the laser's focus causes far-field scatter, and its off-axis motions cause net energy to be deflected from the optical axis. A quadrant photodetector monitors the deflected energy, and position signals are generated from the difference in photocurrents between opposing pairs of quadrant elements.

(Queensgate Instruments Ltd., East Meadow, NY). Built-in capacitance transducers directly monitor displacements of the piezoelectric stage with near-Angstrom resolution. A typical calibration curve for a 0.27-μm-diameter polystyrene particle (Polysciences) is shown in Fig. 2. The linear range is ~300 nm wide and all particles used for LTM stayed within this range. Used below, the slope of this linear region is the positional sensitivity of the laser-tracking signal.

To noninvasively estimate the size of lipid-storage granules, we used the fact that light scattering is very sensitive to particle size, particularly for particles smaller than the wavelength of incident light (van de Hulst, 1981). The positional sensitivity of the laser-tracking signal (see Fig. 2) can be used as a measure of light scattering. As shown in Fig. 3, the positional sensitivity of laser-tracking signals varies with the square of particle size. Because COS7 granules are highly refractile and their images are indistinguishable from polystyrene bead images (see Fig. 5, *inset*), the indices of refraction of the two types of particles must be comparable. Furthermore, light scattering has a very weak dependence on relative index of refraction (van de Hulst, 1981). Without further corrections, we use the calibration curve of Fig. 3 to estimate all granule sizes.

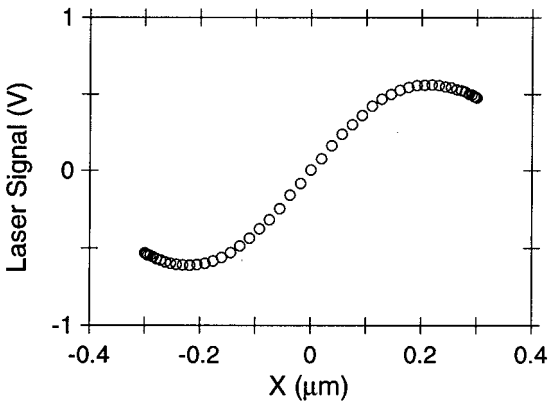

FIGURE 2 Calibrating laser deflection signals. The laser-tracking signal is calibrated by moving particles with a piezoelectric stage. Typical x-axis calibration curve (along $y = 0$) for a polystyrene bead (0.27 μm). For estimating particle sizes, we use the positional sensitivity of the laser signal that is computed as the slope of the calibration curve at its central inflection point.

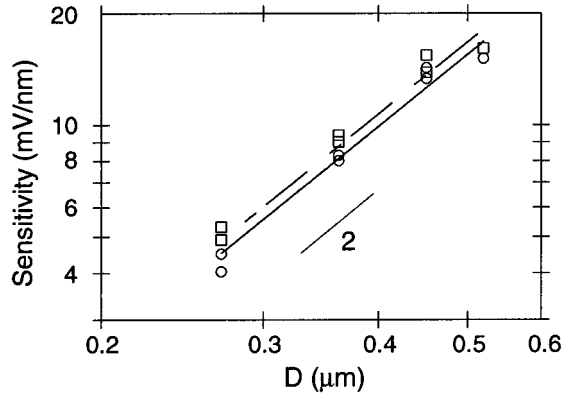

FIGURE 3 Positional sensitivity of laser signal versus the probe diameter. For polystyrene particles of various diameters, the x and y positional sensitivities (*circles* and *squares*, respectively) are shown. The positional sensitivity of the laser signal is computed as the slope of the calibration curve (see Fig. 2) at its central inflection point. All endogenous granules of COS7 fall within the region where positional sensitivity varies quadratically with particle size. For reference, a quadratic slope (power-law of two) and the power-law curve-fitting to both x and y positional sensitivities are shown.

PRINCIPLES

Microrheology from particle trajectory

The Brownian motion of a particle embedded within a filamentous network is directly related to the network's mechanical properties (Xu et al., 1998a; Palmer et al., 1998, 1999; Mason et al., 1997a, b). Phenomenologically, particles exhibit larger motions when their local environments are less rigid or less viscous. As described below, both the amplitude and the time scale are important for calculating mechanical moduli. Calculated over various lag-times, τ, we use the mean-squared-displacement (MSD) $\langle \Delta R^2(\tau) \rangle$ = Average$[(\vec{r}(t+\tau) - \vec{r}(t))^2]$ of the particle's trajectory, $\vec{r}(t)$, to quantify its amplitude of motions over different time scales.

Although the amplitude of particle motions is generally inversely related to the network's mechanical modulus, increases in both rigidity and viscosity will restrict particle motions. To distinguish viscosity from elasticity, the MSD must be measured over a large range of time scales. In purely viscous materials, MSDs of particles vary linearly with lag-times. In purely elastic materials, MSDs are constant, regardless of lag-times. For both of these ideal materials, when deformation frequency is appropriately related to lag-time, the MSD and the magnitude of viscoelastic modulus, $G_d = |G^*|$, are inversely related by a constant factor. However, for viscoelastic materials, a more complex expression is needed to generalize the relationship.

Assuming that inertial effects are negligible, the viscoelastic shear moduli are related to MSD by (Mason and Weitz, 1995):

$$\tilde{G}(s) = s\tilde{\eta}(s) = \frac{2k_BT}{3\pi as\langle \Delta \tilde{R}^2(s) \rangle} \quad (1)$$

where s is the complex Laplace frequency, k_B Boltzmann's constant, T the absolute temperature, a the radius of the particle, and $\langle \Delta \tilde{R}^2(s) \rangle$ the unilateral Laplace transform of the two-dimensional MSD, $\langle \Delta R^2(\tau) \rangle$. For Eq. 1 to be valid there are three criteria that must be satisfied: rigid particle, spherical particle, and that the network is well-approximated as a viscoelastic continuum. Requirements for spherical and rigid particles come from generalizing Stoke's law as a complex function for the particle's resistance to motion, $\tilde{\zeta}(s) = 6\pi a\tilde{\eta}(s)$, within viscoelastic materials. To satisfy the continuum approximation, the particle must be much larger than the pore size of the filamentous network. As discussed later, the lipid-storage granules of COS7 within the lamellae satisfy all of these conditions.

Because numerical Laplace transforms require numerical integration and its associated pitfalls, we use the following two approximations, rather than direct evaluation of Eq. 1. From numerical simulations, both approximations require data spanning at least 2.5 decades of time and frequency for validity (data not shown), and LTM data typically span 5 decades. The complex viscoelastic moduli can be represented in polar notation as

$$\tilde{G}(i\omega) = G'(\omega) + iG''(\omega) = G_d(\omega)\exp(i\delta(\omega)),$$

where

$$G_d(\omega) = |\tilde{G}(i\omega)|$$

and

$$\delta(\omega) = \angle(\tilde{G}(i\omega)) = \arctan(G''(\omega)/G'(\omega)).$$

Using a power-law, or "wedge" (Tschoegl, 1989), approximation of $\langle \Delta R^2(\tau) \rangle$ and its unilateral Fourier transform (Mason et al., 1997b) gives:

$$G_d(\omega) \approx \left. \frac{2k_B T}{3\pi a \langle \Delta R^2(\tau) \rangle \Gamma\left(1 + \frac{d \ln \langle \Delta R^2(\tau) \rangle}{d \ln \tau}\right)} \right|_{\tau = 1/\omega} \quad (2)$$

where Γ is the gamma function. For ideal viscous or elastic materials, where the MSD, $\langle \Delta R^2(\tau) \rangle$, is either linearly related or independent of τ, the gamma function has value of unity ($\Gamma(2) = \Gamma(1) = 1$) and Eq. 2 is exact. Other phenomenological approximation methods are possible (Tschoegl, 1989), but Eq. 2 has performed very well so far (Xu et al., 1998a; Palmer et al., 1998). To extract the phase angle $\delta(\omega)$, we use the deceptively simple approximation derived by Booij and Thoone (1982):

$$\delta(\omega) = \frac{1}{\pi} \int_{-\infty}^{\infty} \frac{d \ln G_d(u)}{d \ln u} \ln \left| \frac{u + \omega}{u - \omega} \right| d \ln u \approx \frac{\pi}{2} \left(\frac{d \ln G_d(u)}{d \ln u} \right)_{u = \omega} \quad (3)$$

which relates the slope of log-log plots (power law) of G_d spectra to the phase angle. With data exceeding 2 decades of frequency bandwidth, Eq. 3 is a highly accurate approximation, and its empirically determined standard deviations never exceed 5% (Booij and Thoone, 1982).

RESULTS

Endogenous granules as probes

In principle, LTM can be a completely noninvasive measurement of cell mechanics. When using endogenous cellular particles, no cell manipulations or deformations are needed. However, the choice of organelles as probes must proceed with rigor. The endogenous particles must be spherical and rigid to satisfy the underlying assumptions of Stokes' law (Eq. 1). Fortunately, COS7 cells are rich with highly refractile granules. Just like polystyrene beads, immobilized granules show no detectable fluctuations beyond the intrinsic noise of our instrumentation (<1 nm, 30 kHz; data not shown). Transmission electron micrographs show that these granules are spherical in fixed cells (Fig. 4). These granules are probably lipid droplets, because they lack any surrounding membrane bilayer. Lipid storage granules are observed in many cell types, and appear as refractile spheres in a light microscope. When using osmium tetroxide, such lipid droplets are intensely stained in electron micrographs (Fawcett, 1981) and appear as in Fig. 4. Furthermore, these COS7 granules are intensely stained with the lipid-droplet specific fluorescent dye, Nile Red (Greenspan et al., 1985), but do not immunostain with endoplasmic reticulum (ER), Golgi, or lysosomal markers (T. Schroer, personal communication). In this paper we restrict the term "endogenous granules" only to refer to these lipid droplets within COS7, and we do not refer to any other organelle.

To demonstrate the appropriateness of endogenous granules as probes, we suspended polystyrene beads and granules partially purified from COS7 into the same gelatin solution. Because granules are frequently indistinguishable from beads by DIC microscopy (see Fig. 5, *inset*), we used fluorescent beads and fluorescence microscopy to identify particles. As shown in Fig. 5, laser-tracking measurements cannot distinguish lipid-storage granules from polystyrene particles; both types of particles give identical viscoelastic spectra for gelatin. By satisfying all prerequisites, these

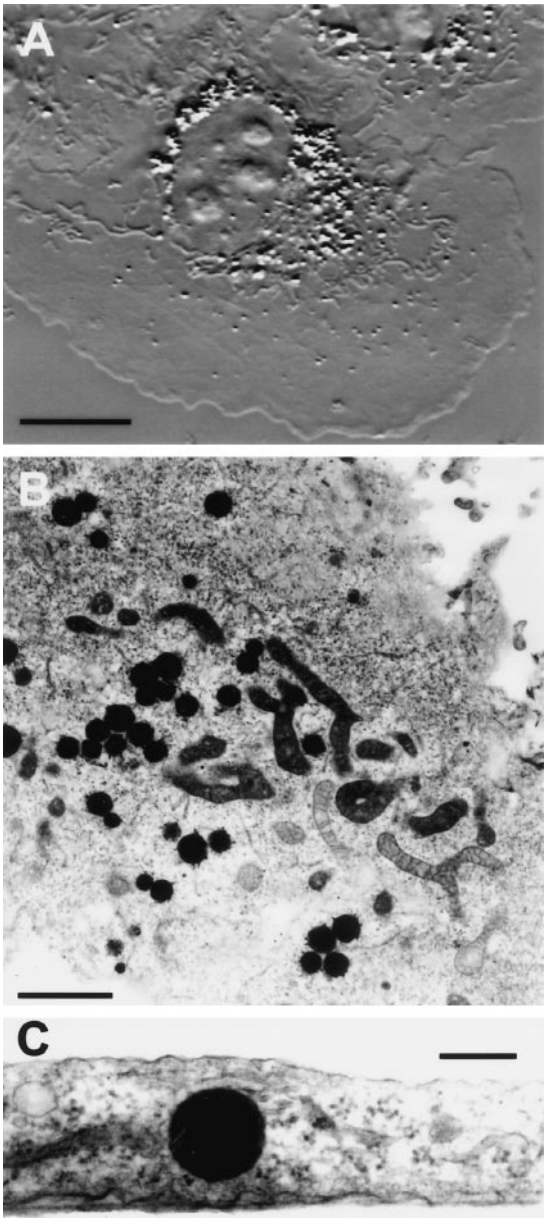

FIGURE 4 Endogenous granules of COS7. (*A*) Video-enhanced DIC image of COS7 cells showing many optically refractile granules distributed throughout the cytoplasm. Scale bar 10 μm. (*B*) Sectioned parallel to the substrate, thin-section electron micrograph of COS7 shows granules intensely stained by uranyl acetate. Scale bar 2 μm. (*C*) Sectioned orthogonally to the substrate, thin-section electron micrograph of COS7. Scale bar 0.2 μm.

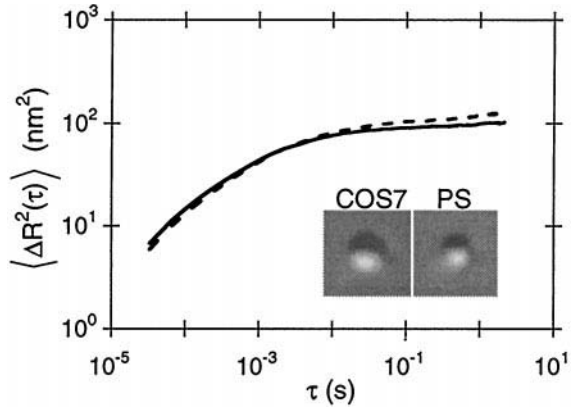

FIGURE 5 LTM of endogenous granules (COS7) and polystyrene (PS) particles co-embedded in gelatin. After lysing COS7 cells by brief sonication, granules and fluorescent polystyrene beads were mixed with molten gelatin (30 mg/ml, 37°C), assembled into slide chambers and allowed to cool to ensnare particles. MSDs were calculated from the trajectories of two adjacent particles in the gel, one a COS7 granule (*dashed line*) and the other a fluorescent microsphere (*solid line*). By laser-tracking sensitivity (see Methods), both particles appear the same size, so MSDs can be compared directly. *Inset*: DIC images of granule and polystyrene particles are indistinguishable.

granules make excellent probes for noninvasive measurements of cellular mechanics.

Viscoelastic nature of cytoplasm

Laser tracking reveals that subcellular particles experience a viscoelastic environment. At three different time scales, Fig. 6 *A* shows the trajectory of a typical lipid-storage granule located in COS7 lamellae. At longer time scales, the trajectory of the granule becomes more restricted. In contrast, diffusion in a purely viscous material should produce a more sparse random walk (see Saxton, 1993). Furthermore, purely viscous diffusion predicts an MSD that is proportional to lag-time, τ. Endogenous granules show subdiffusive behavior at all MSD lag-times (Fig. 6 *B*). Even at the fastest times ($\tau < 1$ ms), the granule experiences the effects of the cytoskeletal network, which never behaves as if purely viscous. For comparison, particles merely tethered by molecular motors show purely viscous behavior on these fast time scales ($0.1 < \tau < 23$ ms; Allersma et al., 1998). At longer time scales ($\tau > 2$ ms), the granule's motions become progressively more constrained, but MSDs never reach a true plateau. Such plateaus would be expected for purely elastic materials. Like lamellar granules, perinuclear granules can also behave subdiffusively, but never purely elastically. Living cytoplasm is clearly a very complex viscoelastic material.

Subcellular mechanics

Although laser-tracking alone indicates viscoelastic behavior, full LTM analysis yields quantitative spectra of cellular

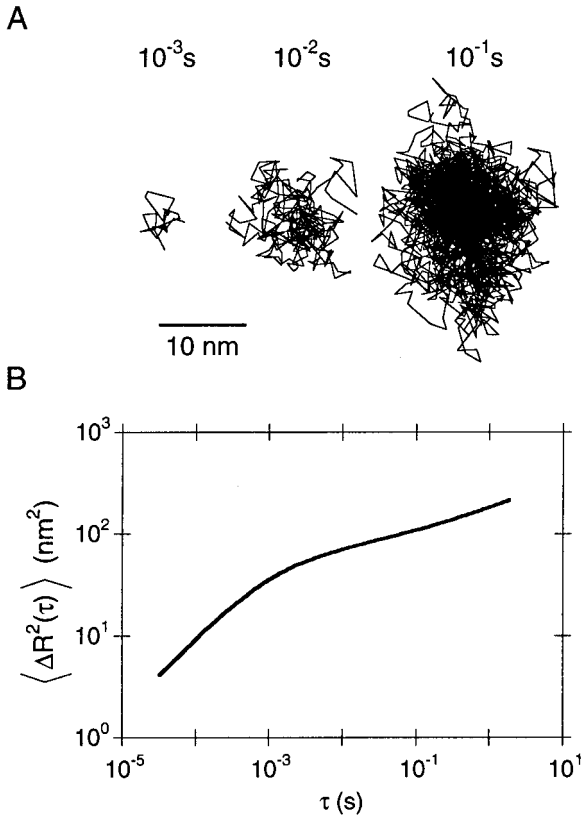

FIGURE 6 Brownian motion of an endogenous granule inside living a cell. (*A*) The trajectory of the endogenous granule over different time scales. (*B*) The mean-squared displacement of the granule's motions.

mechanics. Furthermore, with particles in appropriate locations, LTM can compare the mechanics of subcellular regions. By laser-tracking granules in lamellae and perinuclear regions of cytoplasm (14 cells, 49 different granules), LTM reveals different absolute viscoelastic moduli, G_d, and phase angle, δ, for these two regions (Fig. 7). Spectral data for each granule were averaged from at least five separate acquisitions of data (>20 s total). To make initial estimates, simple morphological rules were sufficient to identify mechanical regions in COS7: perinuclear granules were within a 20-μm radius of the center of a nucleus (average radii of nuclei were 9.2 ± 1.6 μm) and lamellar particles beyond this radius. For LTM, we ignored all granules that were above or below the nucleus, showing large Brownian excursions (>0.2 μm), or undergoing active movements (>0.5 μm). Less than 5% of all granules showed active movement. Although >90% of perinuclear granules showed Brownian excursions that were too large to track by LTM, granules adjacent to the ER and Golgi were more firmly trapped and were used for LTM. No granules within the ER/Golgi networks were used for LTM analysis. At all frequencies, lamellae regions resist particle motions (higher moduli) more than perinuclear regions (Fig. 7). While the moduli of these subcellular regions are significantly differ-

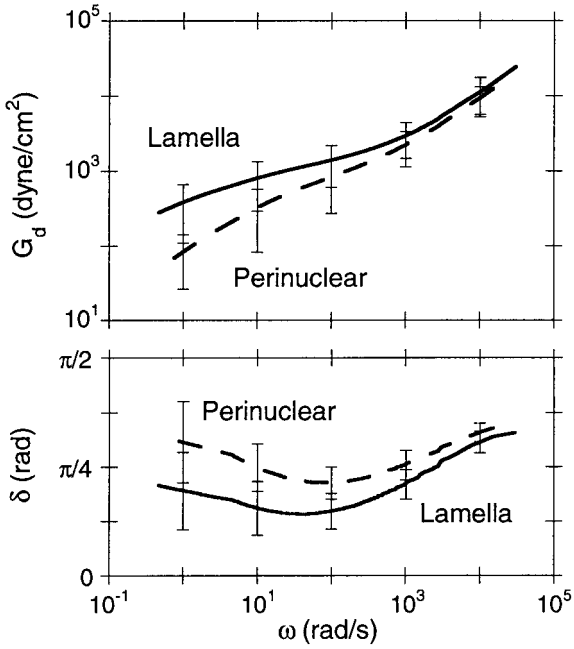

FIGURE 7 Local heterogeneity of cytoplasm. As described in Methods, viscoelastic spectra were calculated from mean-squared displacements of 49 different granules within 14 different cells. As described in the text, subcellular regions were identified by simple morphometric rules, with 11 granules perinuclear and 38 particles in the lamellae. Error bars are standard deviations.

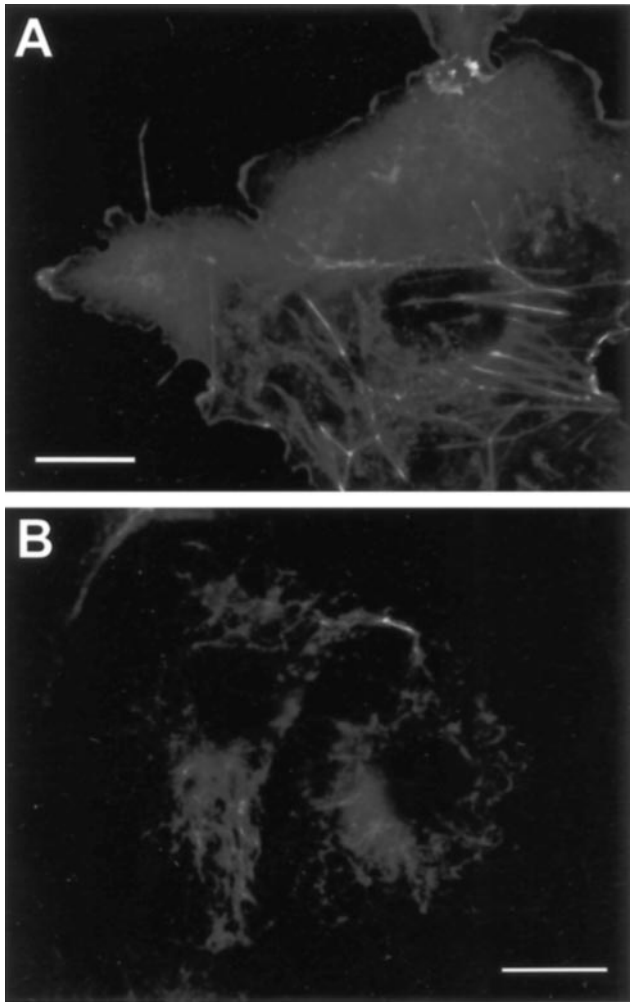

FIGURE 8 Fluorescent staining after LTM measurements. As described in Methods, cells were fixed and stained with (*A*) phalloidin or (*B*) anti-vimentin antibodies. By simple morphometric rules, F-actin was typically most concentrated in lamellae and vimentin in the perinuclear region. Scale bars are 20 μm.

ent at low frequencies ($p < 0.0001$), they converge at higher frequencies (>1000 rad/s). For both subcellular regions, the phase angles suggest viscoelastic behavior at all frequencies. Surprisingly, embedded perinuclear granules of COS7 never exhibit fully liquid-like behavior (i.e. $\delta = \pi/2$), as expected for particles merely tethered by molecular motors (Allersma et al., 1998). Furthermore, they did not show any episodes of directed motion during tracking.

Fixation and fluorescent staining after LTM measurements suggest the sources of viscoelastic behavior. Microtubule immunostaining of COS7 cells was too sparse to explain viscoelastic behavior (data not shown). However, COS7 cells have a very high concentration of vimentin in their perinuclear regions (Fig. 8 *B*). In contrast, fluorescent phalloidin staining for F-actin is greater in lamellae than the perinuclear regions (Fig. 8 *A*). In general, higher phalloidin staining correlated with higher viscoelastic moduli.

Compared to LTM measurements of reconstituted materials such as F-actin (e.g., Fig. 10), cellular measurements have much higher variability in mechanics. Although much of the variability is probably due to spatial heterogeneity, a part of the variability is also due to the dynamics of cytoplasm. Fig. 9 shows the temporal variations in lamellar mechanics as individual granules were monitored over time. Data for reconstituted F-actin networks are included for comparison. For some granules, moduli can vary fourfold and changes persist for many seconds. In contrast, by high-magnification video-enhanced microscopy, COS7 lamellae under these conditions appear quiescent and almost static. Little ruffling or protrusive activity is observed. Because the range of particle motions changes only twofold, these dynamics would be undetectable without the high sensitivity of laser tracking.

Pure F-actin is softer and different from lamellae

Because F-actin staining in COS7 is richest in lamellae, we can use LTM to directly compare their viscoelastic spectra with purified actin. As shown in Fig. 10, LTM of pure F-actin networks at physiological concentrations are ~70-fold softer than COS7 lamellae. By mechanical rheometry and multiple light-scattering, F-actin displays a characteristic plateau in modulus at low frequencies ($\omega < 10$ rad/s;

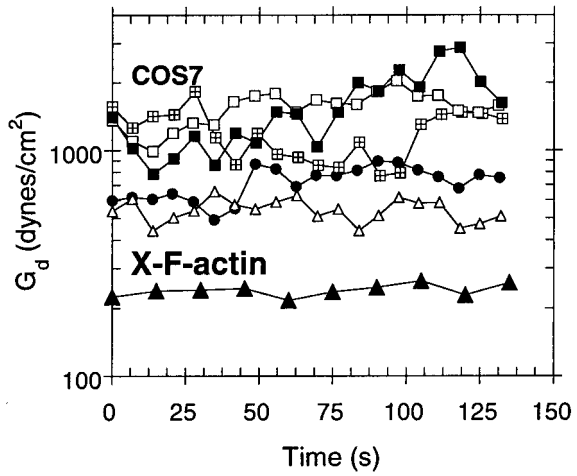

FIGURE 9 Dynamics within apparently quiescent lamellae. Individual granules in the lamellae of COS7 were monitored with LTM over time. Before each LTM acquisition re-calibration of the laser-tracking signal showed no change in instrument response. For comparison, LTM measurements of a polystyrene bead in biotinylated F-actin (12% biotinylated, 15 μM) cross-linked with 0.3 μM avidin is shown (*labeled X-F-actin*). In general, LTM measurements of reconstituted polymers show much less variability than COS7 lamellae.

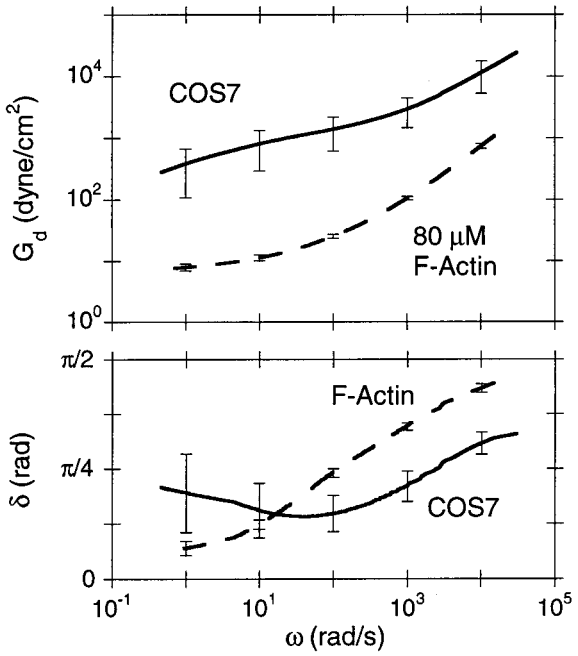

FIGURE 10 Mechanics of F-actin versus COS7 lamellae. Using LTM, viscoelastic spectra were acquired from polystyrene beads in pure F-actin at physiological concentrations (80 μM). Error bars are standard deviations. Compared to COS7 lamellae, there is almost a two-order magnitude difference in absolute viscoelastic moduli. From the viscoelastic phase angle, lamellae are never as liquid-like as F-actin at high frequencies ($\omega >$ 200 rad/s), but F-actin is much more solid-like at low frequencies ($\omega <$ 20 rad/s).

e.g., Janmey et al., 1994). Unlike prior attempts with laser tracking in F-actin (Schnurr et al., 1997), we have succeeded in preserving this low-frequency behavior. Our values for the plateau modulus generally agree with recently published values from other techniques (Palmer et al., 1999; Tang et al., 1999; Xu et al., 1998b).

The viscoelastic phase angle of pure F-actin indicates that it is qualitatively very different from cytoplasm. Pure F-actin exhibits biphasic behavior: solid-like at low frequencies ($\delta < \pi/8$, $\omega < 10$ rad/s) and almost liquid-like at higher frequencies ($\omega > 500$ rad/s). Not purely viscous, this high frequency behavior shows a $\delta \sim 3\pi/8$ relationship ($G_d \sim \omega^{3/4}$) that is characteristic of semiflexible polymers (e.g., Morse, 1998). In contrast, COS7 cytoplasm show little changes in viscoelastic phase angle across frequencies ($\delta \sim \pi/4$). At high frequencies, cytoplasm is both more rigid and more solid-like than F-actin alone. At low frequencies relevant for physiological function, cytoplasm is more rigid, but more liquid-like, than F-actin alone. As discussed later, such qualitative differences are likely due to the dynamics of short-lived cross-linking by actin-binding proteins.

Latrunculin A quickly softens and liquefies quiescent lamellae

The cellular effects of actin-disrupting agents have been amply demonstrated in dynamic cells (e.g., neuronal growth cones; Forscher and Smith, 1988). However, responses from quiescent cells are typically less spectacular. With LTM, we can laser-track the granules before and after pharmacological treatments. As shown in Fig. 11, the environment around a lamellar granule changes dramatically after latrunculin A treatment (~15 min), both softening (5-fold on G_d) and liquefying (2-fold on δ). Results for cytochalasin D are similar (not shown). Brief latrunculin A treatment primarily affects low-frequency behavior, consistent with filament shortening. Dominated by filament-bending modes, high-frequency behavior would be less sensitive to filament lengths (e.g., Morse, 1998). Although dramatic by LTM, such magnitude changes in cellular mechanics are difficult to resolve by other techniques.

DISCUSSION

Laser-tracking microrheology (LTM) is a new, fast technique that can measure the full mechanical complexity of living cytoplasm. Summarized with the mean-squared-displacement function (MSD, $\langle \Delta R^2(\tau) \rangle$), the primary data are the trajectories of embedded particles undergoing restricted Brownian motion. With ~5 decade frequency bandwidth of high-resolution data, we can apply numerical methods so that the MSD yields the viscoelastic modulus and phase angle of the cytoskeletal network around the particle. As discussed later, there are approximations inherent in this

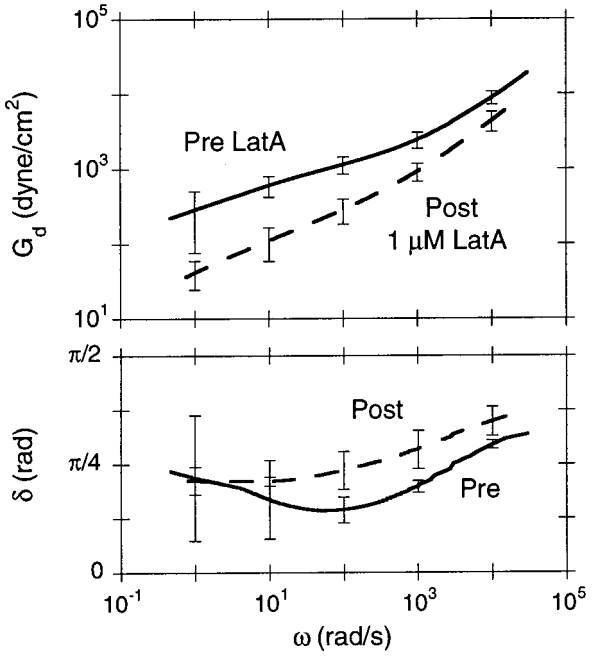

FIGURE 11 Effect of latrunculin A on COS7 lamellae. Lamellar mechanics around each endogenous granule was measured before and after 15-min exposure to 1 μM latrunculin A. Error bars are standard deviations.

method, but endogenous granules in COS7 cells satisfy the requirements for such analysis.

The cytoplasmic viscoelasticity of COS7 cells varies with subcellular region and is dynamic. Phenomenological springs and dashpots are not useful for describing COS7 mechanics because too many parameters would be needed to curve-fit ~5 decades of cellular data. Instead, physiologically relevant low-frequency moduli and phase angles are summarized in Table 1. In rank order, COS7 lamellae, a subset of COS7 perinuclear regions, and pure F-actin are softer and qualitatively very different. Although an F-actin gel is orders of magnitude softer than lamellae, F-actin is necessary for lamellar mechanics because actin-disrupting agents soften lamellae. Even apparently quiescent COS7 cells are dynamic. In as short as 15-s duration, lamellar granules can show changes in local moduli, some as large as fourfold in magnitude.

By offering three unique abilities in microscopic mechanics, LTM provides a new level of mechanical information to cell biology. First, LTM is the only microscopic technique capable of measuring the cytoskeleton's viscoelastic phase angle, $\delta(\omega)$, which is an index of the network's solid-like ($\delta = 0$) or liquid-like ($\delta = \pi/2$) behavior. Second, submillisecond resolution allows LTM to distinguish mere tethering from firm entrapment of particles within the cytoskeletal network. Third, LTM has the spatial and temporal resolution to monitor subtle mechanical changes in otherwise quiescent cells or to monitor fast physiological responses. As an added benefit, LTM provides a new tool to help bridge cell biology and biochemical reconstitution. The same technique used in cells can be used on reconstituted networks and provide high-quality spectra with parsimonious amounts (<20 μl) of protein.

Related techniques

LTM extends the capabilities of two well-known biophysical techniques. Like LTM, fluorescence recovery after photobleaching (FRAP, e.g., Luby-Phelps et al., 1986) and video-based single-particle tracking (VSPT, e.g., Saxton and Jacobson, 1997; Sheetz et al., 1989) can measure diffusion coefficients and mobile fractions. For such measurements of "microviscosity" and permeation, the tracer particles are necessarily smaller than the pores of the mesh. Unlike FRAP and VSPT, laser tracking can also monitor the motions of seemingly stationary particles that are larger than the pores of the network. The subdiffusive motions of such particles reflect the elasticity, as well as the bulk viscosity, of the gel.

In principle, data from VSPT could be analyzed using Eq. 1 to provide viscoelastic spectra. This approach has been applied to DNA solutions (Mason et al., 1997a) and, in a more limited form, to particles bound to microtubule

TABLE 1 Mechanics of living COS7 cells

	RMS Fluctuations (nm)	n	δ (deg)	G_d (dyne/cm^2)	Relative Modulus
F-actin (80 μM)	24.3* (d = 1 μm)	5	23 ± 2°	11 ± 1	1
COS7					
Perinuclear (embedded subset)	15.3	11	45 ± 10°	330 ± 250	29
Lamellae	9.9	38	28 ± 11°	820 ± 520	72
Latrunculin A (1 μM, 15 min)	23.6	3	38 ± 2°	110 ± 53	10

All values of viscoelastic phase angle and absolute moduli were evaluated at 10 rad/s, and all statistics are mean ± standard deviation. Root-mean-squared (RMS) fluctuations were calculated over 4.4 s of each acquisition. F-actin, alone, is very biphasic and behaves liquid-like at higher frequencies ($\delta > 45°$, $\omega > 100$ rad/s). As described in the text, lamellae and perinuclear regions were identified by simple morphological rules.

*Measurements of F-actin used 1 μm beads as probes, so RMS fluctuations of 0.3 μm beads would be at least threefold larger. As described in the text, all measurements of COS7 used endogenous granules (0.3 ± 0.1 μm) as probes.

networks (Caspi et al., 1998). With commercially available equipment, video tracking can monitor multiple particles for motions over great distances with near-nanometer resolution (Kuo et al., 1991). However, the main limitation of video tracking is its slow sampling rate (30 Hz), which can be further compounded by phosphor latency in some tube cameras. With its slow speed, minutes of video tracking are required for any numerical approximations (e.g., Eqs. 2 and 3) to be valid. Without high-frequency information, firmly enmeshed particles cannot be distinguished from merely tethered particles. When phosphor latency is present, video further distorts spectra so that information >3 Hz appears overly viscous and can obscure the elasticity of polymers such as polyethylene oxide (Kuo, unpublished observations). Despite these limitations, VSPT is appealing because of its ease of implementation.

Diffusing wave spectroscopy (DWS) (Mason and Weitz, 1995) is a close relative to LTM. Rather than monitoring a single particle, DWS monitors the relative motions of a high density of particles ($\sim$1% by volume). For greatest sensitivity, the high density ensures that there is multiple light scattering from the particles. Multiply scattered laser light is collected by single-mode optical fibers, and a cross-correlator extracts the autocorrelation of intensity fluctuations. Subsequent curve-fitting yields $\langle \Delta R^2(\tau) \rangle$ for use with Eqs. 1–3. DWS has near-picometer displacement sensitivity at MHz bandwidth, but requires reconstituted networks for seeding with high particle densities. DWS requires curve-fitting to extract $\langle \Delta R^2(\tau) \rangle$, whereas LTM yields $\langle \Delta R^2(\tau) \rangle$ directly and trajectories can be individually compensated for uniform convection or drift. DWS and LTM are complementary techniques, and our data for DWS on F-actin gels are described elsewhere (Palmer et al., 1999).

Although one-dimensional, optical trapping interferometers have sufficient spatiotemporal resolution to monitor Brownian motion. The forces of optical tweezers can be calibrated by measuring the power spectrum of positional fluctuations of trapped particles (Svoboda et al., 1993). Power spectra are curve-fit with a Lorentzian functional form which is consistent with a harmonically bound Brownian particle. Recently, this power-spectrum approach has been generalized to viscoelastic materials, such as F-actin and polyacrylamide, where the functional form is not known (Gittes et al., 1997; Schnurr et al., 1997). Although much more computationally intensive, the power spectrum approach is mathematically equivalent to our MSD approach (Mason et al., 1997b).

Approximations in LTM Analysis

Although LTM offers a wealth of data, the assumptions and approximations inherent in the approach and their implications for living cells deserve careful consideration. For any analysis of fluctuations, the most fundamental assumption is that the system is at steady state and does not have time-varying probabilities for its underlying processes. Such an assumption is appropriate for reconstituted polymers, but living cells are dynamic and can change cytoskeletal structure in seconds. Long observation periods risk spanning different subcellular states, even in apparently quiescent cells (see Fig. 9). Fortunately, LTM can make spectral measurements in as little time as 1 s, so such risks are unlikely.

The particle's translational motion accurately reflects the forces on the particle when two minimal prerequisites are satisfied. First, particles must be more rigid than the surrounding cytoskeletal network. Fluctuations in particle shape would obscure contributions from cytoskeleton. Second, particles must be spherical. With their decreased symmetry, ellipsoidal particles complicate both laser tracking and the numerical analysis in LTM. In COS7, we show that endogenous lipid storage granules fulfill these two simple criteria. Hence, any correlation function, such as the MSD, $\langle \Delta R^2(\tau) \rangle$, will accurately summarize the steady-state forces on rigid, spherical granules in COS7.

To obtain viscoelastic spectra from correlation functions, we must assume that the cytoskeletal network is microscopically uniform. Such a continuum approximation is very good in lamellae where cytoskeletal pores are a small fraction of particle size. In the lamellae, granules are $\sim$10-fold larger than cytoskeletal pores (24–31 nm; Provance et al., 1993; Luby-Phelps et al., 1986, 1987). However, in the perinuclear region, cytoskeletal pores are often comparable in size to granules, if not larger. In borderline situations, LTM analysis would underestimate viscoelastic moduli and overestimate phase angles. In extreme cases, particles would percolate through the pores and exhibit only liquid-like phase angles. However, the perinuclear region is not homogeneous, and exceptions to such generalizations are discussed later.

Implications for cytoarchitecture

Although the actin-rich lamellae of vertebrate cells generally exclude organelles, the exclusion is rarely complete. For the kidney-derived cell line, COS7, spherical granules frequently exist in the lamellae (Fig. 4), despite their general concentration in the perinuclear region. These granules are lipid-storage droplets because they lack lipid bilayers, intensely stained with osmium tetroxide/uranyl acetate, and fluorescently stained with Nile Red. These granules are very rigid, as no internal fluctuations of stationary granules are detectable by our laser instrumentation. Overall, these endogenous granules make ideal probes for noninvasive application of LTM, and frequently exist within lamellae.

Because lamellae are rich in F-actin, mechanics of lamellae should be compared to F-actin. F-actin is clearly important, not only because of its enrichment in lamellae, but because of the rapidity of softening by actin-disrupting agents. However, LTM measurements of pure F-actin net-

works confirm the measurements of many investigators and techniques, ranging from mechanical rheometry (e.g., Tang et al., 1999; Xu et al., 1998b) to diffusing wave spectroscopy (e.g., Palmer et al., 1999; Gisler and Weitz, 1999). Uncross-linked F-actin networks, even at high concentrations, are orders of magnitude too soft to explain cellular mechanics. Cross-linking filaments is sufficient to increase moduli by appropriate magnitudes (e.g., Wachsstock et al., 1994). However, the lifetimes of cross-links between filaments are critical for the qualitative hardening of networks. Long-lived cross-links, such as biotin-avidin, produce "solid" F-actin networks. In contrast, short-lived cross-links not only increase moduli, but also produce higher viscoelastic phase angles, indicative of more liquid-like networks (Wachsstock et al., 1994; Palmer et al., 1998). Compared to F-actin behavior at low frequencies, such cross-linker lifetimes may explain the more liquid-like values of the phase angle observed in COS7.

LTM measurements reveal two new features of mechanics in lamellae. First, despite quiescent appearances, lamellae are dynamic, as well as heterogeneous. Second, by providing the first subcellular estimates of viscoelastic phase angles, LTM shows intermediate levels of liquid-like and solid-like behavior ($\delta \sim \pi/4$) at all frequencies. Because there are no frequencies of solid or liquid behavior, simple spring-and-dashpot models are fundamentally incorrect and merely phenomenological. Even phenomenologically, a system of multiple ($\sim$8) springs and dashpots would be needed to describe cellular viscoelastic spectra across all 5 decades of frequencies.

LTM also reveals a dense viscoelastic subregion near the nucleus. Although most perinuclear granules show large Brownian motions, a subset of these granules is firmly embedded in a relatively rigid viscoelastic material. These granules are often near endoplasmic reticulum and Golgi, which are also rich in the intermediate filament, vimentin. These same regions exclude small fluorescent tracer molecules (Provance et al., 1993; Luby-Phelps et al., 1986, 1987). Because there are no obvious organelles adjacent to the embedded perinuclear granules described here, we suspect that intermediate filaments are responsible for local viscoelasticity. However, additional experiments are needed to identify the source of perinuclear viscoelasticity.

The high-frequency information from laser tracking is critical for confirming the appropriateness of LTM interpretations, particularly in the perinuclear region. Because the perinuclear region is dominated by particles displaying near-percolation behavior, apparently stationary granules may be particles tethered by molecular motors rather than embedded in a viscoelastic matrix. When particles are merely tethered to microtubules, they exhibit diffusive behavior on fast time scales ($0.1 < \tau < 23$ ms; Allersma et al., 1998). If analyzed using Eqs. 1–3, such behavior would appear as viscoelastic phase angle values of $\delta \sim \pi/2$ for frequencies $\omega > 400$ rad/s. None of the embedded perinuclear granules or lamellar granules had any evidence of such "microviscosity." Even though such data cannot exclude the possibility of additional filament-binding by granules, it is clear that the granules are in viscoelastic microenvironments.

Because the biological roles of various subcellular particles are different, their microenvironments are necessarily different. For example, during early phagocytosis, particles recruit actin and actin-binding proteins that should alter local mechanical properties. Depending on content, maturing phagosomes experience different fates and interact with cytoskeleton differently. In COS7, preliminary data show that late phagocytosed polystyrene beads show higher moduli ($\sim$5-fold) than endogenous granules (data not shown). These differences persist despite multiple proliferative passages of bead-containing cells. Because a particle's Brownian motion reflects its microenvironment, beads and granules must have subtly different microenvironments. Identifying the molecular differences in microenvironments requires further study. Indeed, even within the same subcellular region probed with one class of particle, our data indicate a high variability of local mechanics. With such heterogeneity of cytoplasm, the idealized concept of uniform bulk properties is not accurate, but necessary as a starting point for understanding cell structure.

Comparison with other cellular measurements

LTM provides unique information by revealing the full viscoelastic complexity of cytoplasm. It measures the cytoplasm's frequency-dependent modulus and phase angle over a broad range of frequencies. Although other techniques measure a smaller range of frequencies, comparisons to LTM can be restricted to corresponding frequency ranges. In addition, many of these other techniques use ligands that might activate cytoskeletal recruitment (e.g., Plopper and Ingber, 1993) or use large deformations that risk exploring nonlinear and plastic mechanical responses as well as risk spanning multiple subcellular mechanical regions. Such differences complicate comparisons between techniques, but good frequency-limited agreement occurs in methods that closely match LTM conditions (magnetic tweezers, Table 2).

Table 2 summarizes numerical estimates of cell mechanics from a number of techniques. Spanning multiple subcellular domains, most extracellular measurements deform the cortical cytoskeleton and the cytoplasm. In general, extracellular estimates are one to two orders of magnitude larger than intracellular measurements, and numerical values vary by orders of magnitude.

Intracellular measurements appear less disparate. Before LTM, only intracellular measurements using internalized magnetic particles have been reported. Inside murine macrophages, twisting a population of magnetic particles reveal a viscous cytoplasm with only a minor elastic response (Valberg and Albertini, 1985). Because most ($\sim$80%)

TABLE 2 Selected measurements of cell mechanics

Technique	Cell Type	Elasticity (dyne/cm^2)	Viscosity (poise)	Param Model*	Citation
Extracellular or Whole Cell Measurements					
Magnetic twist	endothelial	~20	n.a.	secant	Wang et al., 1993
Micropipette	leukocyte	7.5, 238	330	3	Sung et al., 1988
Mech. rheometer	*D. discoideum*	$G' = 550$	$G'' = 250^{\dagger}$	direct	10 rad/s (Eichinger et al., 1996)
Cell poker	neutrophil	1180	n.a.	secant	Zahalak et al., 1990
AFM	platelet	$(1–50) \times 10^3$	n.a.	Hertz	Radmacher et al., 1996
Microplates	fibroblast	$\sim 10^4$	10^3–10^5	3	Thoumine and Ott, 1997
Spont. retraction	fibroblast	1.7×10^4	4×10^6	2	Ragsdale et al., 1997
Magnetic tweezers	fibroblast	$\sim 3 \times 10^5$	$\sim 2 \times 10^4$	4	Bausch et al., 1998
Intracellular Measurements					
Magnetic twist	macrophage	~150	$\sim 2 \times 10^4$	secant	Valberg and Albertini, 1985
Magnetic tweezers	macrophage	200–7350	2100	4	Bausch et al., 1999
deduced		$G' \sim 1790^{\ddagger}$	$G'' \sim 1182^{\dagger\ddagger}$	*deduced*‡	4 elem. model (10 rad/s)
LTM	epithelial	$G' = 721$	$G'' = 382^{\dagger}$	direct	this work (10 rad/s)

Abbreviations: n.a., not available; AFM, atomic force microscopy; LTM, laser-tracking microrheology.

*Mechanical models for extracting values: the secant method normalizes the apparent force/displacement for the geometry of the mechanical probe. In AFM, the Hertzian model further normalizes for the changing contact area of pyramidal probes. In creep or relaxation methods, estimating viscosity typically uses mechanical spring-and-dashpot models or models that include surface tension, and the number of parameters in the model are listed in this table. In rheometry, dynamic storage (G') and loss (G'') moduli are directly measured.

†Units of G″ are dyne/cm^2.

‡Dynamic storage and loss moduli were calculated from the 4-element mechanical model using the average of measured values (Bausch et al., 1999): $k_0 = 1180$ dyne/cm^2, $k_1 = 2250$ dyne/cm^2, $n_0 = 2100$ poise, and $\tau = 0.218$ s, which lead to a deduced value for $n_1 = 169$ poise.

COS7 granules show large Brownian excursions, comparable population measurements would be similarly soft and liquid-like. Using magnetic tweezers, Bausch et al. (1999) analyzed displacements of individual ferromagnetic particles phagocytosed inside macrophages. The values for these cytoplasmic particles are almost two orders of magnitude smaller than corresponding extracellular particles (Bausch et al., 1998) and are much more variable (elastic shear moduli range 200–7350 dyne/cm^2, with average 3430 $\pm$ 2340 dyne/cm^2). Since Bausch's model with four mechanical elements is not a unique arrangement for phenomenological characterization, numerical estimates from such a model are not directly comparable to other techniques. However, the storage and loss moduli (G' and G'', respectively) can be estimated from the model and can be compared to LTM measurements. Such a calculation is shown in Table 2. Mindful that phagocytosed particles display higher moduli than endogenous granules in COS7 (data not shown), the values from LTM are in good agreement with comparable measurements using magnetic tweezers.

LTM provides a new approach to measuring cellular mechanics and should provide a valuable complement to other cell biological techniques. For cell biology, it has three critical technical advantages: sensitivity, speed, and highly local measurements. Small changes in apparent moduli are readily discerned, and measurements can be accomplished on physiological time scales (within seconds). Because cells are highly heterogeneous, very local measurements are needed for biological relevance. Overall, LTM's ability to bridge biochemical reconstitution and cell biology should provide insights into processes that remodel cytoskeleton.

We thank K. Ganesan for developing and rebuilding the LTM apparatus, and J. McGrath for a careful reading of the manuscript. We also thank A. Palmer and J. Xu for purifying actin, K. Leong for the COS7 cell line, P. Coulombe for vimentin antibodies, and D. Murphy for fluorescence and electron microscopy access and assistance.

This work was supported in part by the Whitaker Foundation (S.C.K.), the National Science Foundation (S.C.K., D.W.), and NASA (S.C.K., D.W.).

REFERENCES

A-Hassan, E., W. F. Heinz, M. D. Antonik, N. P. D'Costa, S. Nageswaran, C. A. Schoenenberger, and J. H. Hoh. 1998. Relative microelastic mapping of living cells by atomic force microscopy. *Biophys. J.* 74: 1564–1578.

Allersma, M. W., F. Gittes, M. J. deCastro, R. J. Stewart, and C. F. Schmidt. 1998. Two-dimensional tracking of ncd motility by back focal plane interferometry. *Biophys. J.* 74:1074–1085.

Bausch, A. R., W. Moller, and E. Sackmann. 1999. Measurement of local viscoelasticity in living cells by magnetic tweezers. *Biophys. J.* 76: 573–579.

Bausch, A. R., F. Ziemann, A. A. Boulbitch, K. Jacobson, and E. Sackmann. 1998. Local measurements of viscoelastic parameters of adherent cell surfaces by magnetic bead microrheometry. *Biophys. J.* 75: 2038–2049.

Booij, H. C., and G. P. J. M. Thoone. 1982. Generalization of Kramers-Kronig transforms and some approximations of relations between viscoelastic quantities. *Rheol. Acta.* 21:15–24.

Caspi, A., M. Elbaum, R. Granek, A. Lachish, and D. Zbaida. 1998. Semiflexible polymer network: a view from inside. *Phys. Rev. Lett.* 80:1106–1109.

Crick, F. H. C., and A. F. W. Hughes. 1950. The physical properties of cytoplasm: a study by means of the magnetic particle methods. *Exp. Cell Res.* 1:37–80.

Eichinger, L., B. Koppel, A. A. Noegel, M. Schleicher, M. Schliwa, K. Weijer, W. Witke, and P. A. Janmey. 1996. Mechanical perturbation elicits a phenotypic difference between *Dictyostelium* wild-type cells and cytoskeletal mutants. *Biophys. J.* 70:1054–1060.

Fawcett, D. W. 1981. The Cell. W. B. Saunders Co., Philadelphia.

Felder, S., and E. L. Elson. 1990. Mechanics of fibroblast locomotion: quantitative analysis of forces and motions at the leading lamellas of fibroblasts. *J. Cell Biol.* 111:2513–2526.

Forscher, P., and S. J. Smith. 1988. Actions of cytochalasins on the organization of actin filaments and microtubules in a neuronal growth cone. *J. Cell Biol.* 107:1505–1516.

Gisler, T., and D. Weitz. 1999. Scaling of the microrheology of semidilute F-actin solutions. *Phys. Rev. Lett.* 82:1606–1609.

Gittes, F., B. Schnurr, P. D. Olmsted, F. C. MacKintosh, and C. F. Schmidt. 1997. Microscopic viscoelasticity: shear moduli of soft materials determined from thermal fluctuations. *Phys. Rev. Lett.* 79:3286–3289.

Greenspan, P., E. P. Mayer, and S. D. Fowler. 1985. Nile Red: a selective fluorescent stain for intracellular lipid droplets. *J. Cell Biol.* 100: 965–973.

Hochmuth, R. M. 1993. Measuring the mechanical properties of individual human blood cells. *J. Biomech. Eng.* 115:515–519.

Hou, L., K. Luby-Phelps, and F. Lanni. 1990. Brownian motion of inert tracer macromolecules in polymerized and spontaneously bundled mixtures of actin and filamin. *J. Cell Biol.* 110:1645–1654.

Janmey, P. A., S. Hvidt, J. Kas, D. Lerche, A. Maggs, E. Sackmann, M. Schliwa, and T. P. Stossel. 1994. The mechanical properties of actin gels. Elastic modulus and filament motions. *J. Biol. Chem.* 269: 32503–32513.

Kuo, S. C., J. Gelles, E. Steuer, and M. P. Sheetz. 1991. A model for kinesin movement from nanometer-level measurements of kinesin and cytoplasmic dynein and force measurements. *J. Cell Sci.* (Suppl. 14): 135–138.

Kuo, S. C., and M. P. Sheetz. 1992. Optical tweezers in cell biology. *Trends Cell Biol.* 2:116–118.

Luby-Phelps, K., P. E. Castle, D. L. Taylor, and F. Lanni. 1987. Hindered diffusion of inert tracer particles in the cytoplasm of mouse 3T3 cells. *Proc. Natl. Acad. Sci. USA.* 84:4910–4913.

Luby-Phelps, K., D. L. Taylor, and F. Lanni. 1986. Probing the structure of cytoplasm. *J. Cell Biol.* 102:2015–2022.

MacLean-Fletcher, S. D., and T. D. Pollard. 1980. Viscometric analysis of the gelation of *Acanthamoeba* extracts and purification of two gelation factors. *J. Cell Biol.* 85:414–428.

Mason, T. G., A. Dhople, and D. Wirtz. 1997a. Concentrated DNA rheology and microrheology. *Mat. Res. Soc. Symp. Proc.* 463:153–158.

Mason, T. G., K. Ganesan, J. H. Van Zanten, D. Wirtz, and S. C. Kuo. 1997b. Particle tracking microrheology of complex fluids. *Phys. Rev. Lett.* 79:3282–3285.

Mason, T. G., and D. A. Weitz. 1995. Optical measurements of frequency-dependent linear viscoelastic moduli of complex fluids. *Phys. Rev. Lett.* 74:1250–1253.

Morse, D. C. 1998. Viscoelasticity of concentrated isotropic solutions of semiflexible polymers. 2. Linear response. *Macromolecules.* 31: 7044–7067.

Nicklas, R. B. 1983. Measurements of the force produced by the mitotic spindle in anaphase. *J. Cell Biol.* 97:542–548.

Palmer, A., T. G. Mason, J. Xu, S. C. Kuo, and D. Wirtz. 1999. Diffusing wave spectroscopy microrheology of actin filament networks. *Biophys. J.* 76:1063–1071.

Palmer, A., J. Xu, and D. Wirtz. 1998. High-frequency viscoelasticity of crosslinked actin filament networks measured by diffusing wave spectroscopy. *Rheol. Acta.* 37:97–106.

Petersen, N. O., W. B. McConnaughey, and E. L. Elson. 1982. Dependence of locally measured cellular deformability on position on the cell, temperature, and cytochalasin B. *Proc. Natl. Acad. Sci. USA.* 79: 5327–5331.

Plopper, G., and D. E. Ingber. 1993. Rapid induction and isolation of focal adhesion complexes. *Biochem. Biophys. Res. Commun.* 193:571–578.

Provance, D. W., Jr., A. McDowall, M. Marko, and K. Luby-Phelps. 1993. Cytoarchitecture of size-excluding compartments in living cells. *J. Cell Sci.* 106:565–577.

Radmacher, M., M. Fritz, C. M. Kacher, J. P. Cleveland, and P. K. Hansma. 1996. Measuring the viscoelastic properties of human platelets with the atomic force microscope. *Biophys. J.* 70:556–567.

Ragsdale, G. K., J. Phelps, and K. Luby-Phelps. 1997. Viscoelastic response of fibroblasts to tension transmitted through adherens junctions. *Biophys. J.* 73:2798–2808.

Saxton, M. J. 1993. Lateral diffusion in an archipelago. Single-particle diffusion. *Biophys. J.* 64:1766–1780.

Saxton, M. J., and K. Jacobson. 1997. Single-particle tracking: applications to membrane dynamics. *Annu. Rev. Biophys. Biomol. Struct.* 26: 373–399.

Schmidt, C. E., A. F. Horwitz, D. A. Lauffenburger, and M. P. Sheetz. 1993. Integrin-cytoskeletal interactions in migrating fibroblasts are dynamic, asymmetric, and regulated. *J. Cell Biol.* 123:977–991.

Schnurr, B., F. Gittes, F. C. MacKintosh, and C. F. Schmidt. 1997. Determining microscopic viscoelasticity in flexible and semiflexible polymer networks from thermal fluctuations. *Macromolecules.* 30: 7781–7792.

Sheetz, M. P., S. Turney, H. Qian, and E. L. Elson. 1989. Nanometre-level analysis demonstrates that lipid flow does not drive membrane glycoprotein movements. *Nature.* 340:284–288.

Spudich, J. A., and S. Watt. 1971. The regulation of rabbit skeletal muscle contraction. I. Biochemical studies of the interaction of the tropomyosin-troponin complex with actin and the proteolytic fragments of myosin. *J. Biol. Chem.* 246:4866–4871.

Sung, K.-L. P., C. Dong, G. W. Schmid-Schönbein, S. Chien, and R. Skalak. 1988. Leukocyte relaxation properties. *Biophys. J.* 54:331–336.

Svoboda, K., C. F. Schmidt, B. J. Schnapp, and S. M. Block. 1993. Direct observation of kinesin stepping by optical trapping interferometry. *Nature.* 365:721–727.

Tang, J. X., P. A. Janmey, T. P. Stossel, and T. Ito. 1999. Thiol oxidation of actin produces dimers that enhance the elasticity of the F-actin network. *Biophys. J.* 76:2208–2215.

Thoumine, O., and A. Ott. 1997. Time scale dependent viscoelastic and contractile regimes in fibroblasts probed by microplate manipulation. *J. Cell Sci.* 110:2109–2116.

Tschoegl, N. W. 1989. The Phenomenological Theory of Linear Viscoelastic Behavior: An Introduction. Springer-Verlag, New York.

Valberg, P. A., and D. F. Albertini. 1985. Cytoplasmic motions, rheology, and structure probed by a novel magnetic particle method. *J. Cell Biol.* 101:130–140.

van de Hulst, H. C. 1981. Light Scattering by Small Particles. Dover Publications, Inc., New York.

Wachsstock, D. H., W. H. Schwarz, and T. D. Pollard. 1994. Cross-linker dynamics determine the mechanical properties of actin gels. *Biophys. J.* 66:801–809.

Wang, N., J. P. Butler, and D. E. Ingber. 1993. Mechanotransduction across the cell surface and through the cytoskeleton. *Science.* 260: 1124–1127.

Xu, J., A. Palmer, and D. Wirtz. 1998a. Rheology and microrheology of semiflexible polymer solutions: actin filament networks. *Macromolecules.* 31:6486–6492.

Xu, J., W. H. Schwarz, J. A. Kas, T. P. Stossel, P. A. Janmey, and T. D. Pollard. 1998b. Mechanical properties of actin filament networks depend on preparation, polymerization conditions, and storage of actin monomers. *Biophys. J.* 74:2731–2740.

Zahalak, G. I., W. B. McConnaughey, and E. L. Elson. 1990. Determination of cellular mechanical properties by cell poking, with an application to leukocytes. *J. Biomech. Eng.* 112:283–294.